

Optimising primordial non-Gaussianity measurements from galaxy surveys

Eva-Maria Mueller,^{1*} Will J. Percival,¹ Rossana Ruggeri¹

¹*Institute of Cosmology & Gravitation, University of Portsmouth, Dennis Sciama Building, Portsmouth, PO1 3FX, UK*

Accepted XXX. Received YYY; in original form ZZZ

ABSTRACT

Galaxy clustering data from current and upcoming large scale structure surveys can provide strong constraints on primordial non-Gaussianity through the scale-dependent halo bias. To fully exploit the information from galaxy surveys, optimal analysis methods need to be developed and applied to the data. Since the halo bias is sensitive to local non-Gaussianity predominately at large scales, the volume of a given survey is crucial. Consequently, for such analyses we do not want to split into redshift bins, which would lead to information loss due to edge effects, but instead analyse the full sample. We present an optimal technique to directly constrain local non-Gaussianity parametrised by $f_{\text{NL}}^{\text{loc}}$, from galaxy clustering by applying redshift weights to the galaxies. We derive a set of weights to optimally measure the amplitude of local non-Gaussianity, $f_{\text{NL}}^{\text{loc}}$, discuss the redshift weighted power spectrum estimators, outline the implementation procedure and test our weighting scheme against Lognormal catalogs for two different surveys: the quasar sample of the Extended Baryon Oscillation Spectroscopic Survey (eBOSS) and the emission line galaxy sample of the Dark Energy Spectroscopic Instrument (DESI) survey. We find an improvement of 30 percent for eBOSS and 6 percent for DESI compared to the standard Feldman, Kaiser & Peacock weights, although these predictions are sensitive to the bias model assumed.

Key words: cosmology: observations - inflation - large-scale structure of Universe

1 INTRODUCTION

Primordial non-Gaussianity (PNG) is one of the most promising probes to distinguish between different models of inflation, a theory to describe an era of exponential expansion of the very early universe that was first introduced to solve problems within the Big Bang model. Inflation can solve the horizon problem as well as the flatness problem, and can also explain the origin of structure formation through the creation of initial fluctuations. Currently, the best constraints on PNG are provided by measurements of the cosmic microwave background (CMB) with the Planck satellite (Planck Collaboration et al. 2016).

Even though current constraints from large scale structure (LSS) data (i.g. Ross et al. (2013)) are weaker than the CMB results, future galaxy surveys have the potential to significantly improve upon these limits (see e.g. Carbone et al. (2008); Fedeli et al. (2011); Giannantonio et al. (2012); de Putter & Doré (2014); Camera et al. (2015); Ferraro & Smith (2015); Byun & Bean (2015); Becker et al. (2012); Giannantonio et al. (2012); Raccanelli et al. (2015)) by constraining

the scale dependent halo bias induced by PNG (Dalal et al. 2008; Matarrese & Verde 2008; Slosar et al. 2008; Desjacques & Seljak 2010). Upcoming spectroscopic surveys such as the extended Baryon acoustic Oscillation Spectroscopic Survey (eBOSS) (Zhao et al. 2016), the Euclid mission (Amendola et al. 2013), as well as the Dark Energy Spectroscopic Instrument (DESI) (Font-Ribera et al. 2014) survey are expected to constrain the amplitude of local non-Gaussianity, $f_{\text{NL}}^{\text{loc}}$, around a few (from here on we will drop the subscript ‘loc’ for simplicity); however, to achieve that level of accuracy, analysing techniques need to be optimised to fully exploit the LSS information. Indeed, most galaxy redshift survey analyses fall short of their expected results predicted using Fisher Matrix techniques.

It was recently realised (Zhu et al. 2015) that that some of the missing signal is lost because analyses are generally performed after splitting a galaxy sample into redshift shells. Instead, they proposed adopting an analysis strategy that relies on assigning weights to the galaxies over a broad redshift range, showing that this retains more information provided that the weights take the redshift evolution of the underlying physical theory into account. This has the potential to notably improve cosmological constraints from LSS surveys.

* E-mail: eva-maria.mueller@port.ac.uk

Zhu et al. (2015) focussed on optimising LSS surveys for BAO measurements, and their method was shown to work using mock catalogs in Zhu et al. (2016). In subsequent work, redshift weights were derived to constrain modified gravity through Redshift Space Distortions (RSD) in Ruggeri et al. (2017). These weights can be interpreted as a natural extension of the Feldman, Kaiser & Peacock (FKP) weights (Feldman et al. 1994), that balance galaxies according to their number densities, for the case that the cosmological observables of interest evolve with time. If the underlying physical theory is independent of redshift then the weights reduce to the standard FKP weights. In the future, multiple galaxy surveys will cover a large redshift range, $0 < z < 3$, making the redshift weighting technique particularly efficient as well as necessary to avoid information loss due to edge effects and disjoint bins. Furthermore, the computational time can be reduced significantly since the redshift weighting technique only requires a single analysis instead of measuring each redshift bin separately. Redshift weighting also removes the need to define an effective redshift of a survey by providing measurements with known variation over the redshift range.

In this paper, we derive and assess the redshift weights for optimising LSS surveys for local f_{NL} measurements. Avoiding redshift binning is particularly relevant for non-Gaussianity measurements since the effect of the scale dependent bias dominates on very large scales. Breaking the survey into redshift bins (for example, considering the clustering in bins of width $\Delta z = 0.1$), removes large-scale clustering signal. For the correlation function it is clear that such binning removes pairs of galaxies, where galaxies lie in different bins. For the power spectrum, the binning introduces a window function, correlating large-scale modes, and decreasing the effective number of modes.

The paper is organised as follows: In Section 2 we summarise modelling of the power spectrum as well as the observable effects of non-Gaussianity on the power spectrum. We introduce the concept of redshift weighting in Section 3.1 and derive the optimal weights for f_{NL} measurements in Section 3.2. We outline the procedure of how to apply the weights to the data in Section 3.3. In Section 3.4 we discuss the modelling of the redshift weighted power spectrum and in Section 4 we estimate the improvement of using f_{NL} weights compared to FKP weights by simulating the redshift weighted power spectrum estimators using Lognormal catalogs. Finally, Section 5 contains the discussion of our results and conclusions.

2 PHYSICAL MODEL

In this Section we provide a brief summary of the scale dependent halo bias induced by non-Gaussianity. In the framework of local non-Gaussianity, i.e. a type of non-Gaussianity that only depends on the local value of the potential, the primordial potential can be parametrised as (Komatsu & Spergel 2001; Gangui et al. 1994)

$$\Phi = \phi + f_{\text{NL}}(\phi^2 - \langle \phi^2 \rangle) \quad (1)$$

where ϕ is a gaussian random field and f_{NL} describes the amplitude of the quadratic correction to the potential. The potential can then be related to the density field via $\delta(k) =$

$\alpha(k)\Phi(k)$, with

$$\alpha(k) = \frac{2k^2 T(k) D(z)}{3\Omega_m} \frac{c^2}{H_0^2} \frac{g(0)}{g(\infty)} \quad (2)$$

with the transfer function $T(k)$, the linear growth factor $D(z)$ normalised to be unity at $z = 0$, the matter density today Ω_m , the speed of light c and the Hubble parameter today H_0 . The factor $g(\infty)/g(0)$, with $g(z) = (1+z)D(z)$, arises due to our normalisation of $D(z)$ and can be omitted if $D(z)$ is normalised to equal the scale factor during the matter dominated era. Here we are using the CMB convention for f_{NL} assuming Φ is the primordial potential. Note that some authors have previously adopted a "LSS convention" that assumes Φ is extrapolated to $z = 0$, with $f_{\text{NL}}^{\text{LSS}} = g(\infty)/g(0) f_{\text{NL}}^{\text{CMB}} \approx 1.3 f_{\text{NL}}^{\text{CMB}}$. We do not do this as we consider it unnecessary and potentially confusing.

The scale dependent halo bias $\Delta b(k)$ in the local Ansatz is then given by (Dalal et al. 2008; Slosar et al. 2008)

$$\Delta b(k) = 2(b-p) f_{\text{NL}} \frac{\delta_{\text{crit}}}{\alpha(k)} \quad (3)$$

where $\delta_{\text{crit}} = 1.686$ and $1 < p < 1.6$ depending on the type of tracer. Here we follow Slosar et al. (2008) assuming $p = 1$ for luminous red galaxies (LRGs) and emission line galaxies (ELGs) and $p = 1.6$ for quasars.

The total bias, including local non-Gaussianity is then $b_{\text{tot}} = b + \Delta b(k)$.

In the limit of the plane parallel approximation, the linear matter power spectrum P in redshift space is (Kaiser 1987)

$$P(k, \mu) = (b_{\text{tot}} + f\mu^2)^2 P_M(k) \quad (4)$$

where f is the linear growth rate, μ is the cosine of the angle between the wavevector \mathbf{k} and the line of sight and $P_M(k)$ is the linear matter power spectrum. The effect of f_{NL} is included in the definition of the total bias. From an observational point of view it is more convenient to consider the power spectrum multipoles defined as

$$P_l(k) = \frac{2l+1}{2} \int_{-1}^1 d\mu P(k, \mu) \mathcal{L}_l(\mu) \quad (5)$$

where $\mathcal{L}_l(\mu)$ are the Legendre polynomials, instead of the linear power spectrum given by equation (4). Even though the power spectrum is fully defined by its first three moments at linear order, only the monopole

$$P_0(k) = \left(b_{\text{tot}}^2 + \frac{2}{3} f b_{\text{tot}} + \frac{1}{5} f^2 \right) P_M(k) \quad (6)$$

as well as the quadrupole

$$P_2(k) = \left(\frac{4}{3} b_{\text{tot}} f + \frac{4}{7} f^2 \right) P_M(k) \quad (7)$$

depend on the bias. Therefore we focus our analysis to these multipoles.

3 OPTIMAL WEIGHTS

3.1 Redshift weights

Following the procedure outlined in Ruggeri et al. (2017) and Zhu et al. (2016) we can derive the optimal redshift weights

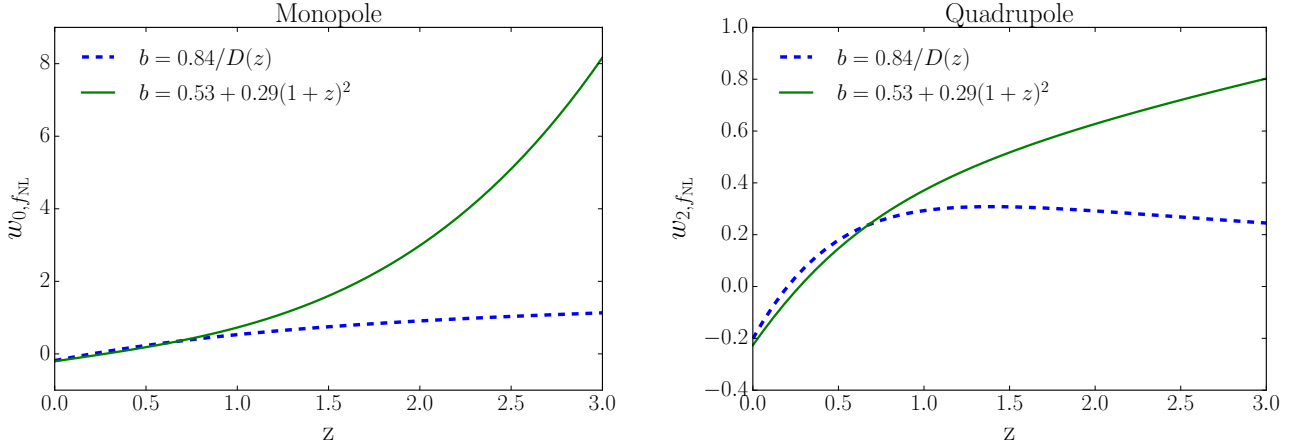


Figure 1. Optimal redshift weights for local non-Gaussianity, f_{NL} , measurements as a function of redshift for the power spectrum monopole [left panel] and quadrupole [right panel]. Blue dashed lines assume a bias model $b(z) = 0.53 + 0.29(1+z)^2$ and $p = 1.6$ referring to quasars as tracer of the underlying matter density, while green lines are for $b(z) = 0.84/D(z)$ and $p = 1.0$, referring to ELGs. The assumptions on the fiducial value of f_{NL} have an negligible effect on the weights. For these plots we assume a fiducial of $f_{\text{NL}} = 0$

by maximising the Fisher information matrix F defined as

$$F_{ij} \equiv \left\langle \frac{\partial^2 \mathcal{L}}{\partial \theta_i \partial \theta_j} \right\rangle, \quad (8)$$

with the likelihood function \mathcal{L} and the parameters θ_i . Assuming a Gaussian likelihood, the fisher matrix for a single parameter of the weighted data set can be calculated as

$$F_{ii} = \frac{1}{2} \left(\frac{\mathbf{w}^T C_{,i} \mathbf{w}}{\mathbf{w}^T C \mathbf{w}} \right)^2 + \frac{(\mathbf{w}^T \mu_{,i})^2}{\mathbf{w}^T C \mathbf{w}} \quad (10)$$

with the covariance matrix C , the mean μ , the weights \mathbf{w} and the index $,i$ denoting the partial derivative $\partial/\partial\theta_i$ (see e.g. Tegmark et al. 1997; Vogelej & Szalay 1996).

The first term in equation (10) vanishes assuming the covariance matrix is known and independent of the cosmological parameters. The second term is maximised for

$$\mathbf{w}^T = C^{-1} \mu_{,i}. \quad (11)$$

Defining $w_i = \mu_{,i}^T$ as well as $d\mathcal{W} \equiv C^{-1}$ the weights for parameter θ_i can be written as

$$\mathbf{w} = w_i d\mathcal{W}. \quad (12)$$

The factor $d\mathcal{W}$ takes the statistical uncertainty of the observable into consideration whereas w_i factors in the redshift evolution of the theoretical model. The normalisation of the weights is arbitrary and does not affect the cosmological constraints. We choose the normalisation,

$$N_i = \int w_i d\mathcal{W} \quad (13)$$

leading to normalised weights $\hat{\mathbf{w}}$ defined as

$$\hat{\mathbf{w}} \equiv \frac{1}{N_i} w_i d\mathcal{W}. \quad (14)$$

Note first, that the index i refers to the same cosmological parameter but does not imply Einstein summation and second, that our normalisation differs from the one in Zhu et al. (2016) by a factor of w_i .

3.2 Redshift weights for local non-Gaussianity

For the power spectrum $P(k)$, the inverse covariance matrix in each redshift slice can be approximated by

$$d\mathcal{W} \equiv C^{-1} = \left(\frac{\bar{n}}{\bar{n}P + 1} \right)^2 dV \quad (15)$$

depending on the galaxy density \bar{n} as well as the survey volume dV . Since in this analysis we are interested in using measurements of the power spectrum monopole and quadrupole to constrain the non-Gaussianity parameter f_{NL} , the part of weights referring to the redshift evolution of f_{NL} are given by

$$w_{l,f_{\text{NL}}} = \frac{\partial P_l}{\partial f_{\text{NL}}}. \quad (16)$$

The total weights

$$\mathbf{w} = w_{l,f_{\text{NL}}} d\mathcal{W} \quad (17)$$

are then a combination of the volume factor $d\mathcal{W}$ and the f_{NL} weights. In the following we will use the term "redshift weights" to refer to $w_{l,f_{\text{NL}}}$ but one should keep in mind that the total weights also include the volume factor $d\mathcal{W}$. For $w_i = 1$ the weights reduce to the commonly used FKP weights. However, if one is interested in a theory that is more sensitive at high redshifts, for instance, more total weight will be given to galaxies at higher redshifts than in the case of FKP weights.

Using equation (2) and equation (3) together with equation (6), the weight of the monopole reads as

$$w_{0,f_{\text{NL}}} = \left(2b_{\text{tot}} + \frac{2}{3}f \right) \frac{\partial b_{\text{tot}}}{\partial f_{\text{NL}}} P_M(k, z) \quad (18)$$

and furthermore assuming a fiducial value for $f_{\text{NL,fd}} = 0$ simplifies to

$$w_{0,f_{\text{NL}}} = \left(2b + \frac{2}{3}f \right) 2(b-p) \frac{\delta_{\text{crit}}}{\alpha(k, z)} P_M(k, z). \quad (19)$$

Factoring out the explicit redshift dependency as $\alpha(k, z) = \alpha(k, z_0)D(z)$ and $P_M(k, z) = P_M(k, z_0)D(z)^2$ as

well as normalising the weights according to equation (13), the normalised weights can be written independent of the wavevector k . Without the loss of generality, the weights can be redefined as

$$\hat{w}_{0,f_{\text{NL}}} = \frac{1}{N_{0,f_{\text{NL}}}} w_{0,f_{\text{NL}}} \quad (20)$$

where

$$w_{0,f_{\text{NL}}} = \left(b + \frac{1}{3}f\right) (b-p)D(z) \quad (21)$$

$$N_{0,f_{\text{NL}}} = \int w_{0,f_{\text{NL}}} d\mathcal{W}. \quad (22)$$

Similarly the quadrupole weight can be defined as

$$w_{2,f_{\text{NL}}} = \frac{4}{3}f(b-p)D(z). \quad (23)$$

It should be emphasised the scale independence of these weights significantly simplifies their application (see Section 3.3).

Fig. 1 shows the weight for the monopole $w_{0,f_{\text{NL}}}$ [left panel] and the quadrupole $w_{2,f_{\text{NL}}}$ [right panel] as a function of redshift z assuming a bias of $b(z) = 0.53 + 0.29(1+z)^2$ (blue dashed lines) and $p = 1.6$ as well as $b(z) = 0.84/D(z)$ and $p = 1$ (green lines), bias models previously proposed for eBOSS quasars (Zhao et al. 2016) and DESI ELGs (DESI Collaboration et al. 2016) respectively. The weights at low redshifts, $z < 0.75$, are similar for both, but deviate for higher redshifts due to increasing differences in the bias models, with a strong high-redshift bias leading to larger weights at high redshifts. In general, the f_{NL} weights are also larger for higher redshifts since the f_{NL} model is also sensitive to the redshift evolution of the the growth rate.

3.3 Implementation procedure

The implementation procedure was outlined in Zhu et al. (2015) analysing the real space correlation function as well as in Ruggeri et al. (2017) for the power spectrum in Fourier space. For completeness, we summarise some of the key-points here. The redshifts weights can be applied to the data and randoms as an extension of the usual FKP weighting scheme following the prescription of Feldman et al. (1994),

$$w_{\text{FKP}} = \frac{1}{1 + \bar{n}(z)P(k_0)} \quad (24)$$

where $\bar{n}(z)$ is the mean number density at the galaxies's redshift z , and k_0 is commonly assumed to be approximately the BAO scale. The redshift dependent weights are applied in the following way: In real space, each galaxy pair (or pair of randoms) is weighted by $w_{l,f_{\text{NL}}}$ as well as w_{FKP}

$$\widetilde{XY} = \sum_z w_{l,f_{\text{NL}}} w_{\text{FKP}}^2 XY \quad (25)$$

where $\widetilde{XY} = \{DD, DR, RR\}$ refer to the data-data, data-random and random-random pairs of the sample. The standard Landy & Szalay (1993) estimator

$$\xi_{l,f_{\text{NL}}} = \frac{\widetilde{DD} - 2\widetilde{DR} + \widetilde{RR}}{RR} \quad (26)$$

can then be used to calculate the weighted correlation function, where RR are the unweighted random-random pairs.

In Fourier space the procedure is similar. Each galaxy

is weighted by a product of FKP weight and the f_{NL} specific weights as derived in Section 3.1

$$w = \sqrt{w_{\text{FKP}} \times w_{l,f_{\text{NL}}}}. \quad (27)$$

Note, that even though we derived the weights within the framework of the power spectrum, following the assumption that the clustering evolves over larger scales than those being measured, we can approximate the weights applied to the galaxies as the root of the power spectrum weights $w_g = \sqrt{w_P}$.

3.4 Modelling the weighted power spectrum

The model to be fitted to the measured, weighted power, also depends on the weights. i.e. we need both the data and model to be sensitive to the same redshifts. We model the theoretical weighted power spectrum multipoles by compressing them into the redshift direction as

$$P_{l,w}(k) \equiv \frac{1}{N_i} \int d\mathcal{W}(z) w_{l,i}(z) P_l(k, z) \quad (28)$$

with

$$w_{\text{unweighted}} = 1 \quad (29)$$

$$w_{0,f_{\text{NL}}} = \left(b + \frac{1}{3}f\right) (b-p)D(z) \quad (30)$$

$$w_{2,f_{\text{NL}}} = \frac{4}{3}f(b-p)D(z) \quad (31)$$

with the normalisation N_i given by the equation (13).

In general, the theoretical power spectrum includes a convolution with the survey window function. However, considering the galaxy power spectrum as an evolving quantity requires a redefinition of the survey window function (for details see Ruggeri et al., in prep.).

4 TESTING THE REDSHIFT WEIGHTS

In order to test the weights, we generate an ensemble of mock catalogues, based on overdensities drawn from a Lognormal distribution (Coles & Jones 1991). Lognormal-random fields were used for convenience because they approximate the present-day non-linear fluctuation field, and they obey the physical limit $\delta > -1$, which means that they can be Poisson sampled to provide a galaxy distribution with shot-noise and sample variance matching those expected. Although both the assumptions of a Lognormal overdensity field and Poisson-sampled galaxies are crude approximations, they are fit for our purpose of testing the weights.

We generate 10,000 mock catalogues in redshift shells of $\delta z = 0.025$ with the number densities, redshift range, sky coverage and bias model as expected for the eBOSS quasar sample and DESI ELGs. A summary of the survey specifications can be found in Table 1. We assume a box size of $L = V^{1/3}$ with the volume referring to the shell of a given survey calculated as

$$V(z) = \frac{4\pi}{3} f_{\text{sky}} (\chi(z_{\text{max}})^3 - \chi(z_{\text{min}})^3) \quad (32)$$

with the sky coverage fraction f_{sky} and the comoving distance χ . Within each redshift shell we assume no density gradient, simplifying our analysis to avoid a detailed modelling of survey window function. The simulations assume a

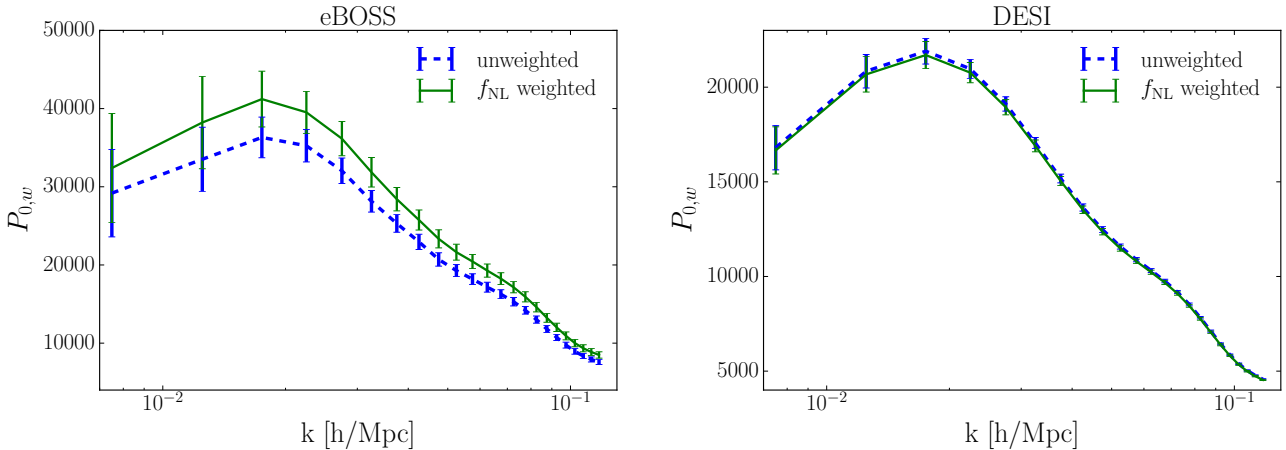


Figure 2. Redshift weighted power spectrum monopole for eBOSS [left panel] and DESI [right panel]. Blue dashed lines correspond to the ‘unweighted’ (or FKP)-weighted monopole (assuming $w_0 = 1$) and green lines represent the f_{NL} -weighted monopole. Details on the survey assumptions are summarised in Tab. 1.

Table 1. We are modelling the eBOSS quasar sample and the DESI ELG sample with the number of galaxies given in Tabel 2 of Zhao et al. (2016) and Table 2.3 in DESI Collaboration et al. (2016) respectively. We are not considering the complete surveys but rather select specific samples to highlight the range of results that can be expected for different survey specification.

survey	tracer	redshift range	sky coverage	bias model
eBOSS	Quasars	$0.6 < z < 2.2$	7,500 deg ²	$b(z) = 0.53 + 0.29(1+z)^2$
DESI	ELGs	$0.6 < z < 1.8$	14,000 deg ²	$b(z) = 0.84/D(z)$

flat Λ CDM cosmology with $\Omega_m = 0.3$, $\Omega_b = 0.045$, $h = 0.7$, $n_s = 1.0$, $\sigma_8 = 0.8$ and $f_{\text{NL}} = 0$ as our fiducial cosmology. We compute the spherically averaged power-spectrum monopole in 23 bins of width $\Delta k = 0.005$ h/Mpc from 0.005 h/Mpc $< k < 0.12$ h/Mpc using

$$P_0(k, z) = \frac{3}{2} \sum |\tilde{\delta}(k)|^2 \mathcal{L}_0(\mu(k)) \quad (33)$$

where $\mathcal{L}_0(\mu)$ is the 0th order Legendre polynomial and $|\tilde{\delta}(k)|^2$ is the squared modulus of the Fourier transform of the overdensity $\delta(r)$ at position r and the sum is over all wavevectors in the range $|k| \pm \Delta k/2$ (see e.g., Pearson et al. 2016). For each mock we then calculate the weighted and unweighted power spectra via equation (28).

In the following analysis we only consider constraints from the monopole as a proof of concept and do not consider constraints from the quadrupole since most of the information on f_{NL} is contained in the monopole (Ross et al. 2013). For each mock the weighted power spectrum is then calculated using equation (28). We calculate the covariance matrix as

$$C_{ij} = \frac{1}{N_m - 1} \sum_{n=1}^{N_m} [d_n(k_i) - \bar{d}(k_i)] [d_n(k_j) - \bar{d}(k_j)] \quad (34)$$

where N_m is the total number of mocks, $d_n(k)$ is the power spectrum monopole from the n th mock.

Fig. 2 shows the f_{NL} -weighted and ‘unweighted’ power spectrum monopole for eBOSS [left panel] and DESI [right panel]. The effect of the f_{NL} -weights is greater for eBOSS due to the adaption of a bias model that evolves more strongly with redshift as well as due to the larger redshift

range of the survey. Note, that the normalisation factor for both surveys is different.

The redshift weighting scheme takes the redshift evolution of the underlying theory into account, potentially shifting the weights towards regions with higher noise in the clustering signal. Therefore, applying redshift weights does not automatically lead to higher signal to noise in the power spectrum itself. Instead, redshift weighting leads to the observable that can constrain the underlying theory the most. In the case of local non-Gaussianity, more weight is given to galaxies at higher redshifts despite the larger statistical uncertainty at these redshifts, because the effect of f_{NL} on the powers spectrum is greater at higher redshifts. Fig. 3 depicts the noise-to-signal as a function of scale for the f_{NL} -weighted and ‘unweighted’ power spectrum monopole for DESI [left panel], as well as the difference of the redshift weighted power spectrum for $f_{\text{NL}} = 10$ and $f_{\text{NL}} = 0$ over the noise [right panel]. Even though the N/S is larger for the f_{NL} -weighted power spectrum, it has a greater capability to constrain f_{NL} than the FKP-weighted power spectrum because it is more sensitive to the f_{NL} .

To get an estimate on the error achievable on a measurement of f_{NL} from both surveys, we calculate the χ^2 surface

$$\chi^2 = (\vec{m} - \vec{d})^T C^{-1} (\vec{m} - \vec{d}) \quad (35)$$

where \vec{d} is the data vector calculated from the mocks and \vec{m} is the model vector. For both surveys we can then calculate the expected likelihood. For eBOSS we find an uncertainty on f_{NL} of $\sigma(f_{\text{NL}}) = 21.63$ at 68% C.L. for the FKP-weighted

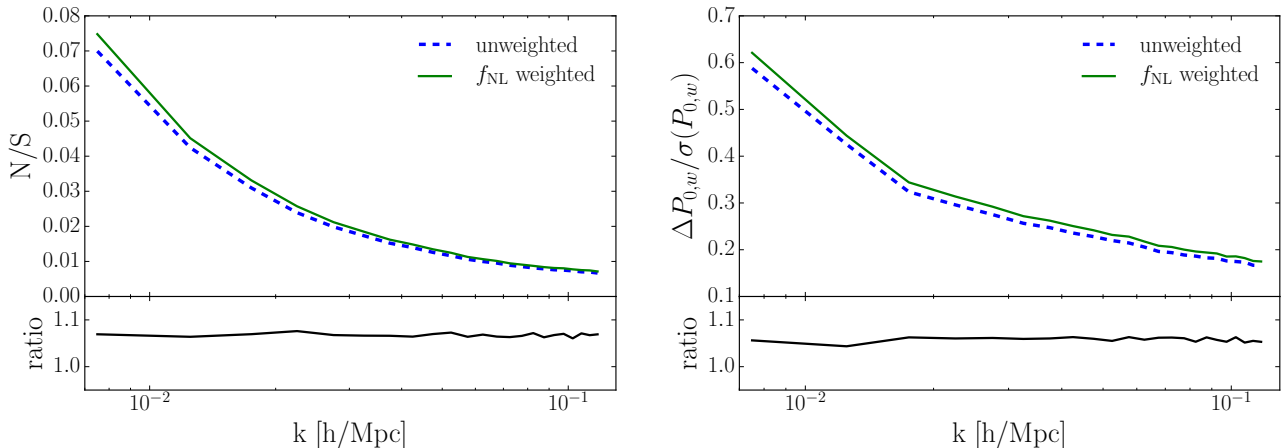


Figure 3. Noise-to-signal of the weighted power spectrum monopole [left panel] and the difference of the weighted power spectrum assuming $f_{\text{NL}} = 10$ and $f_{\text{NL}} = 0$ over the noise, $\Delta P_{0,w}/\sigma(P_{0,w}) = (P_{0,w}(f_{\text{NL}} = 10) - P_{0,w}(f_{\text{NL}} = 0))/\sigma(P_{0,w})$, [right panel]. Blue dashed lines refer to the 'unweighted' power spectrum monopole and green lines to the f_{NL} -weighted monopole. The lower panel shows the ratio between the 'unweighted' and f_{NL} -weighted case. Even though the unweighted monopole has a higher level of noise, the sensitivity to f_{NL} is higher for the f_{NL} -weighted monopole and with that the capacity to constrain to f_{NL} .

case and $\sigma(f_{\text{NL}}) = 16.66$ for the f_{NL} -weighting scheme, an improvement of 30%. The improvement for DESI is slightly lower at around 6%. Our analysis currently uses a scale-dependent FKP weight (i.e. P is allowed to vary with k in the weights). If the FKP weight were fixed, as is often assumed when analysing data for simplicity, then we would expect less good constraints on f_{NL} because of increased cosmic variance and/or shot noise. We would also have a different fractional improvement from the redshift weights, with the improvement increasing if the FKP weights are fixed for $P(k)$ with k on larger scales: those where the f_{NL} signal is stronger and the redshift-weights more effective. For example if the FKP weight is fixed at $k_0 = 0.0475$ the improvement increases to 42% for eBOSS.

The Fisher matrix forecasts for eBOSS quasars are $\sigma(f_{\text{NL}}) = 15.74$ (Zhao et al. 2016) with fixing the bias. The redshift weighting technique yields results closer to the predicted uncertainty compared to the unweighted analysis. We do not quite reach the Fisher forecast accuracy because we only consider the monopole and assume a slightly smaller k -range. The Fisher forecasts for DESI are $\sigma(f_{\text{NL}}) = 3.8$ (Font-Ribera et al. 2014), yet these constraints are for the full DESI survey and not just the ELG sample.

The difference between the improvement for eBOSS and DESI from adding the new weights is driven by the range of bias assumed across the sample under consideration, and so will not be fully known for DESI until the survey starts. Even so, this analysis is a proof of principle that the f_{NL} -redshift weighting can lead to stronger constraints on f_{NL} than a simple FKP-weighted power spectrum.

5 CONCLUSIONS

The scale dependent bias is a strong probe of non-Gaussianity and upcoming LSS surveys will put tight constraints on the amplitude of the primordial fluctuations, f_{NL} . Since these surveys cover large redshift ranges, redshift

weighting, a new analysing technique that does not rely on binning in redshift slices, provides a promising way of fully exploiting LSS information. Redshift weighting is in particular important for studying the primordial universe since non-Gaussianity alters large scales more strongly than small scales. Not splitting the sample into small redshift slices therefore increases the effective number of relevant scales modes that are included in any analysis. Indeed, applying redshift weights will be crucial to reach the accuracy predicted by Fisher forecasts, which implicitly assume that all of the information is extracted, in effect assuming optimised weights are used.

The optimal weights we have derived to measure f_{NL} balance sample variance, shot noise and the redshift evolution of the scale dependent halo bias induced by non-Gaussianity. The weights depend on the properties of the galaxy sample through the evolving bias of the sample. As the bias is generally increasing with redshift, we end up weighting galaxies at high redshift more strongly than at low redshifts, even if the signal-to-noise of the clustering signal is weaker.

We assessed the potential of the f_{NL} weights using mock catalogs generated though a Lognormal code simulating the upcoming eBOSS and DESI surveys. We find that the uncertainty on f_{NL} is minimised when applying the f_{NL} redshift weights, yielding an improvement of 6% up to 30% for DESI and eBOSS respectively compared to analysing an FKP-weighted power spectrum.

There are a few caveats to our analysis: First, the redshift weights to optimally measure local non-Gaussianity depend strongly on the assumed galaxy bias. If the fiducial bias model is inaccurate, then the weights will not be optimal and lead to looser constraints on f_{NL} than expected. However, the redshift weighted power spectrum will still be unbiased. Second, for tracers with no strongly evolving bias the underlying theory is only mildly redshift dependent limiting the overall improvement of the redshift weighting technique. In general, the improvement from the f_{NL} -weighting increases

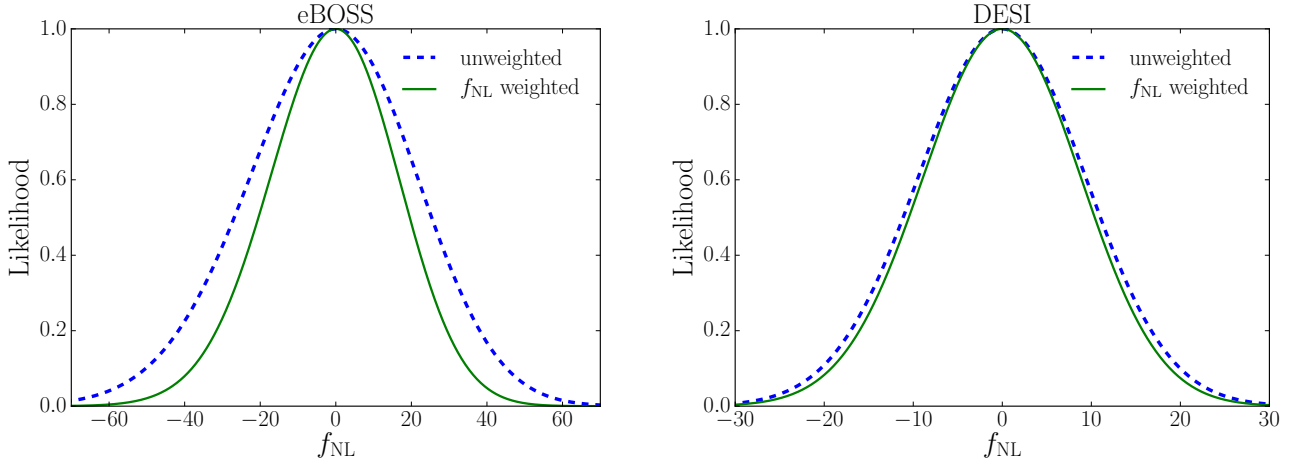


Figure 4. Projected likelihood for f_{NL} measurements from eBOSS quasars [left panel] and DESI ELGs [right panel] for an ‘unweighted’ (green lines) and f_{NL} -weighted (blue dashed lines) power spectrum monopole. The redshift weighting technique can improve the constraints on f_{NL} by 30% for eBOSS quasars and 6% for DESI ELGs. The improvement is larger for eBOSS due to the strong redshift evolution of the assumed bias model as well as a larger redshift range.

with the redshift range of the survey but also depends on the tracer of the sample, with the improvement being stronger where the range of bias across a sample is larger.

We have discussed the potential of redshift weighting to constrain f_{NL} for eBOSS and DESI, but there are also other future surveys for which this technique is highly relevant, for instance the Euclid mission (Amendola et al. 2013) and SPHEREx (Doré et al. 2014). Euclid is a space based, spectroscopic survey of H α -selected emission line galaxies with galaxies in redshift range range $0.7 < z < 2.0$, expected to constrain local non-Gaussianity in addition to BAO and RSD measurements. SPHEREx is a all-sky spectroscopic satellite survey covering a very wide redshift range that was particularly designed to measure non-Gaussianity. It has an evolving redshift accuracy up to $\sigma_z/(1+z) < 0.2$ with low redshifts being more accurately measured than high redshifts. However, we expect the lower redshift accuracy not to be problematic when applying the redshift weights as long as the uncertainty in redshift is taking into account as an additional contribution to the covariance when calculating the weights.

In this work, we have only considered weights optimised to measure non-Gaussianity in the local framework. We leave the study of weights for more complex models, such as equilateral or orthogonal shapes, models with non-zero running of f_{NL} , or shapes with specific angle dependency for future work. Additionally, a natural extension of this work is to apply the redshift weighting technique to multiple tracer samples, therefore combining the optimal redshift weights with weights designed to optimally exploit the additional information through multi tracer methods (Pearson et al. 2016; Hamaus et al. 2011).

ACKNOWLEDGEMENTS

We thank Alkistis Pourtsidou and Fangzhou Zhu for insightful discussions and comments. EM, RR and WJP acknowledge support from the European Research Council through

the Darksurvey grant 614030. WJP also acknowledges support from the UK Science and Technology Facilities Council grant ST/N000668/1 and the UK Space Agency grant ST/N00180X/1.

REFERENCES

- Amendola L., et al., 2013, *Living Reviews in Relativity*, **16**, 6
 Becker A., Huterer D., Kadota K., 2012, *J. Cosmology Astropart. Phys.*, **12**, 034
 Byun J., Bean R., 2015, *J. Cosmology Astropart. Phys.*, **3**, 019
 Camera S., Santos M. G., Maartens R., 2015, *MNRAS*, **448**, 1035
 Carbone C., Verde L., Matarrese S., 2008, *ApJ*, **684**, L1
 Coles P., Jones B., 1991, *Mon. Not. Roy. Astron. Soc.*, **248**, 1
 DESI Collaboration et al., 2016, preprint, ([arXiv:1611.00036](https://arxiv.org/abs/1611.00036))
 Dalal N., Doré O., Huterer D., Shirokov A., 2008, *Phys. Rev. D*, **77**, 123514
 Desjacques V., Seljak U., 2010, *Classical and Quantum Gravity*, **27**, 124011
 Doré O., et al., 2014, preprint, ([arXiv:1412.4872](https://arxiv.org/abs/1412.4872))
 Fedeli C., Carbone C., Moscardini L., Cimatti A., 2011, *MNRAS*, **414**, 1545
 Feldman H. A., Kaiser N., Peacock J. A., 1994, *ApJ*, **426**, 23
 Ferraro S., Smith K. M., 2015, *Phys. Rev. D*, **91**, 043506
 Font-Ribera A., McDonald P., Mostek N., Reid B. A., Seo H.-J., Slosar A., 2014, *J. Cosmology Astropart. Phys.*, **5**, 023
 Gangui A., Lucchin F., Matarrese S., Mollerach S., 1994, *ApJ*, **430**, 447
 Giannantonio T., Porciani C., Carron J., Amara A., Pillepich A., 2012, *MNRAS*, **422**, 2854
 Hamaus N., Seljak U., Desjacques V., 2011, *Phys. Rev. D*, **84**, 083509
 Kaiser N., 1987, *MNRAS*, **227**, 1
 Komatsu E., Spergel D. N., 2001, *Phys. Rev. D*, **63**, 063002
 Landy S. D., Szalay A. S., 1993, *ApJ*, **412**, 64
 Matarrese S., Verde L., 2008, *ApJ*, **677**, L77
 Pearson D. W., Samushia L., Gagrani P., 2016, *MNRAS*, **463**, 2708
 Planck Collaboration et al., 2016, *A&A*, **594**, A17
 Raccanelli A., Doré O., Dalal N., 2015, *J. Cosmology Astropart. Phys.*, **8**, 034

- Ross A. J., et al., 2013, *MNRAS*, **428**, 1116
- Ruggeri R., Percival W. J., Gil-Marín H., Zhu F., Zhao G.-B., Wang Y., 2017, *MNRAS*, **464**, 2698
- Slosar A., Hirata C., Seljak U., Ho S., Padmanabhan N., 2008, *J. Cosmology Astropart. Phys.*, **8**, 031
- Tegmark M., Taylor A. N., Heavens A. F., 1997, *ApJ*, **480**, 22
- Vogeley M. S., Szalay A. S., 1996, *ApJ*, **465**, 34
- Zhao G.-B., et al., 2016, *MNRAS*, **457**, 2377
- Zhu F., Padmanabhan N., White M., 2015, *MNRAS*, **451**, 236
- Zhu F., Padmanabhan N., White M., Ross A. J., Zhao G., 2016, *MNRAS*, **461**, 2867
- de Putter R., Doré O., 2014, preprint, ([arXiv:1412.3854](https://arxiv.org/abs/1412.3854))

This paper has been typeset from a $\text{\TeX}/\text{\LaTeX}$ file prepared by the author.